NANO LETTERS

pubs.acs.org/NanoLett

Electrospun Metal Nanofiber Webs as High-Performance Transparent Electrode

Hui Wu,[†,§] Liangbing Hu,[†,§] Michael W. Rowell,[†] Desheng Kong,[†] Judy J. Cha,[†] James R. McDonough,[†] Jia Zhu,[‡] Yuan Yang,[†] Michael D. McGehee,[†] and Yi Cui*[,†]

[†]Department of Material Science and Engineering and [‡]Electrical Engineering, Stanford University, Stanford, California 94305

ABSTRACT Transparent electrodes, indespensible in displays and solar cells, are currently dominated by indium tin oxide (ITO) films although the high price of indium, brittleness of films, and high vacuum deposition are limiting their applications. Recently, solution-processed networks of nanostructures such as carbon nanotubes (CNTs), graphene, and silver nanowires have attracted great attention as replacements. A low junction resistance between nanostructures is important for decreasing the sheet resistance. However, the junction resistances between CNTs and boundry resistances between graphene nanostructures are too high. The aspect ratios of silver nanowires are limited to ~100, and silver is relatively expensive. Here, we show high-performance transparent electrodes with copper nanofiber networks by a low-cost and scalable electrospinning process. Copper nanofibers have ultrahigh aspect ratios of up to 100000 and fused crossing points with ultralow junction resistances, which result in high transmitance at low sheet resistance, e.g., 90% at 50 Ω/sq. The copper nanofiber networks also show great flexibility and stretchabilty. Organic solar cells using copper nanowire networks as transparent electrodes have a power efficiency of 3.0%, comparable to devices made with ITO electrodes.

KEYWORDS Metal nanofibers, transparent electrodes, flexible electronics, solar cells

Transparent electrodes, which provide electrical contact to the active layer and allow light to pass through, are ubiquitously used in displays and solar cells with increasingly large industry demands. Sheet resistance (R_s) and optical transmittance (T) are two key parameters that determine the applications of transparent electrodes. Different types of devices demand different levels of R_s and T. For example, high-performance touch screens stringently require high T (>95%) but tolerate an R_s of 400−600 Ω/sq.[1] For solar cells and large area displays, R_s needs to be less than 20 Ω/sq to avoid undesired voltage drops and Joule heating during device operation.[2,3] Traditionally, indium tin oxide (ITO) has been widely used as a standard transparent electrode in various types of optoelectronic devices.[4] Due to the constantly increasing demand of ITO for consumer electronics and the low abundance of In, the price of ITO has continually increased throughout the past decade. In addition, ITO thin fims are too brittle to be used in flexible applications.[5,6] Therefore, there has been much effort both in industry and in academia to find a replacement for ITO.[6] Emerging candidates are carbon nanotubes (CNT) and graphene.[7−12,36] Since 2004, steady improvements have been made in the research and development of transparent electrodes based on such nanoscale carbon-based materials. However, a sheet resistance of 100−1000 Ω/sq at 80% optical transmittance in the visible range, achievable in these carbon-based materials, is still too high,[7−10] especially for use in solar cells. More recently, metal nanostructures such as copper nanogrids and solution processed silver nanowires have been developed, with R_s of 10−20 Ω/sq at 80% transparency;[13−18] however, there are multiple limitations. Copper nanogrids require costly lithography steps and are difficult to be scaled up. In solution processed silver nanowire networks, the lengths of the nanowires are typically less than 10 μm, and the use of a polymer surfactant results in charge transport barriers which limit the conductivity.[15,17] It has been demonstrated that longer metal nanowires could lead to better transparent electrode performance.[17]

Electrospinning is currently the most powerful technique that allows fabrication of nanoscale continuous ultralong fibers.[19,20] It employs a strong electrical field to draw very fine (typically on the micro- or nanoscale) fibers from a liquid source (in the schematic illustrated in the left column of Figure 1a). Electrospinning has been explored as a fast and efficient process to fabricate continuous one-dimensional (1D) nanomaterials composed by polymers, oxides, carbon, and, more recently, metals.[19−23] Herein, we introduce electrospinning as a new fabrication method with low cost and high scalability for high-performance copper nanofiber transparent electrodes. The right column of Figure 1a shows a schematic of the Cu nanofiber network fabrication process. In step 1, precursor nanofibers with copper acetate disolved in poly(vinyl acetate) (PVA) are electrospun onto a glass substrate, the fibers have diameters of around 200 nm (supplementary Figure S1 in Supporting Information). In step 2, polymer nanofibers with copper precursors are heated at 500 °C in air for 2 h to remove all the polymer components and the nanofibers are transformed to dark brown CuO

* To whom correspondence should be addressed, yicui@stanford.edu.

§ These authors contributed equally to this work.

Received for review: 08/3/2010
Published on Web: 08/25/2010

DOI: 10.1021/nl102725k | *Nano Lett.* **2010,** *10,* 4242–4248

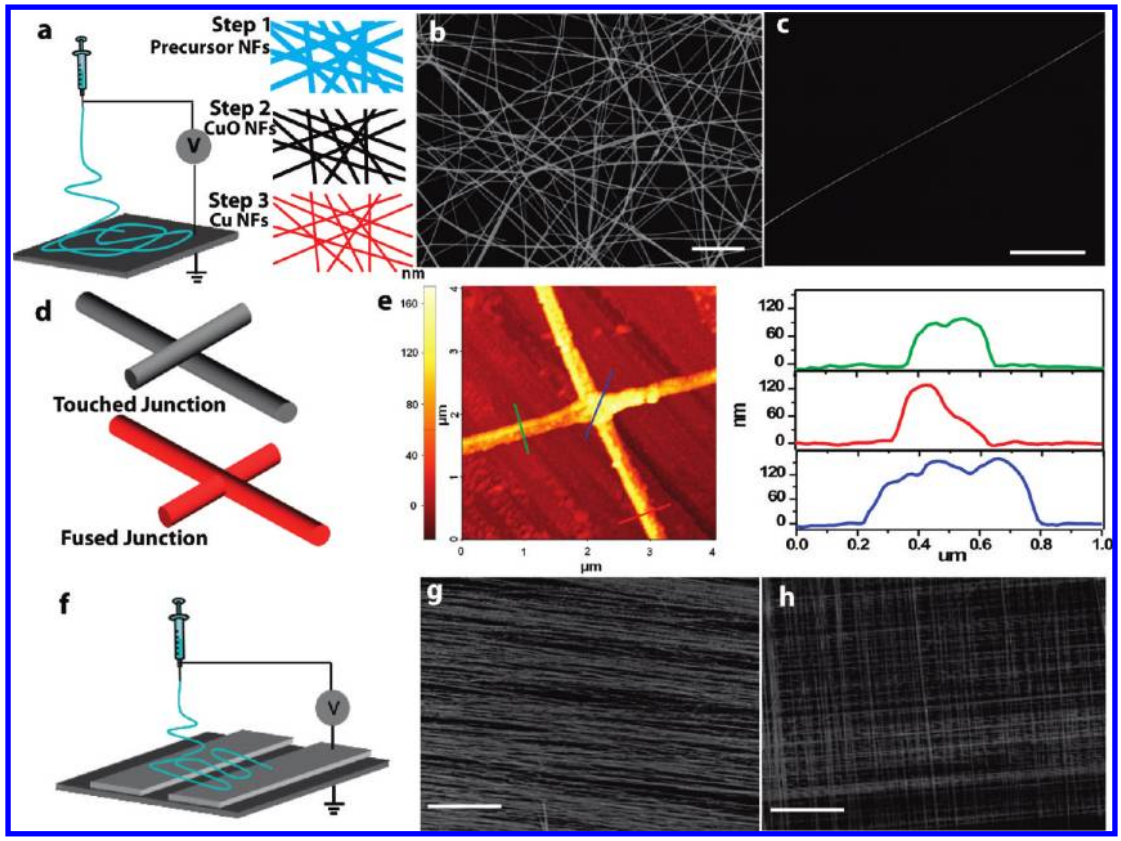

FIGURE 1. Fabrication and characterization of Cu nanofibers. (a) Schematic of materials preparation method. Left column: Schematic of an electrospinning setup, shown without a syringe pump. Right column: the fabrication process of Cu nanofibers. In the first step, $CuAc_2$/PVA composite fibers were prepared by electrospinning. In step 2, the fibers were calcinated in air to get CuO nanofibers. In step 3, the CuO nanofibers were reduced to Cu nanofibers by annealing in an H_2 atmosphere. (b) SEM image of Cu nanofibers synthesized by electrospinning. Scale bar = 10 μm. (c) SEM image showing the continuous structure of a Cu nanofiber, indicating a length that can easily exceed 100 μm. Scale bar = 20 μm. (d) Schematic of junctions between solution-processed Ag nanowires (upper) and electropsun Cu nanofibers (down). (e) AFM image of a junction between two nanofibers. The curved lines show the heights of two nanofibers and the cross junction, respectively. (f) Schematic of modified electrospinning setup, oriented nanofibers can be collected on the gaps between two parallel electrodes. (g, h) SEM images of Cu nanofibers with controlled orientations: (g) uniaxially aligned arrays, (h) patterned grids. Scale bar = 20 μm.

nanofibers. In step 3, CuO nanofibers are reduced into red Cu nanofibers after annealing in an H_2 atmosphere at 300 °C for 1 h (supplementary Figure S2 (Supporting Information) shows the color change of nanofibers after annealing).

Figure 1b presents a scanning electron microscopy (SEM) image of the synthesized Cu nanofiber networks with diameters of ~100 nm. It clearly shows that the Cu nanofibers preserve the morphologies of the original polymer nanofibers. The average diameters of Cu nanofibers can be controlled within the range of 50−200 nm by adjusting electrospinning conditions such as the polymer solution viscosity and the spinning voltage. The area density of Cu nanofibers can be controlled by the electrospinning duration. The as-synthesized Cu nanofibers are polycrystalline with little CuO on the surface, as confirmed by transmission electron microscopy (TEM, supplementary Figure S3 in Supporting Information), selected-area electron diffraction (SAED, supplementary Figure S3 inset, Supporting Information), energy-dispersive X-ray spectroscopy (EDS, supplementary Figure S4, Supporting Information), and powder X-ray diffraction (XRD, supplementary Figure S5, Supporting Information).

The metal nanofibers made by electrospinning have several attractive characteristics for use as excellent transparent electrodes. First, each copper nanofiber is extremely long. In principle, electrospinning produces one continuous fiber to cover the entire surface.[19] In reality, there can be a few breaking points generated during processing. Our Cu nanofibers are found to be continuous for more than 1 cm with diameters of ~100 nm, resulting in extremely high aspect ratios above 100000. Figure 1c shows a 100 μm segment of a single continuous Cu nanofiber. Cu nanofibers provide around 2−3 orders of magnitude higher aspect ratios than other 1D nanomaterials for transparent electrodes (e.g., carbon nanotubes and silver nanowires).[7,9,15,17] The percolation theory for 1D sticks predicts that the percolation threshold, N_c, dramatically decreases as the length of the sticks increases[24]

Because the nanofiber lengths are on the order of a centimeter rather than a micrometer, the percolation critical

$$l\sqrt{\pi N_c} = 4.236 \quad (1)$$

DOI: 10.1021/nl102725k | *Nano Lett.* **2010,** *10,* 4242–4248

density is only $\sim 5.7 \times 10^{-8}/\mu m^2$, which is $\sim 10^8$ times lower than networks of CNTs or Ag NWs.[7,15]

Second, Cu nanofiber networks have ultralow junction resistances due to the unique nanofiber formation process. During the chemical transformation of polymer fibers to CuO nanofibers, thermal heating melts the polymer nanofibers, which merge the two fibers into the same identity at the cross junction point and remove any junction interface (as schematically shown in Figure 1d). The soldered cross joints remain during the CuO to Cu transformation. Supplementary Figure S6 (Supporting Information) shows SEM images of cross junctions between two Cu nanofibers, indicating the melted cross junctions. The fused joint nature of cross junctions is further confirmed by atomic force microscopy (AFM, Figure 1e). The heights of the two single Cu nanofibers are 120 and 90 nm, respectively, and the height of the cross junction is 125 nm, which is close to that of a single fiber and much lower than the sum of the heights of the two nanofibers (210 nm). This result indicates that two Cu nanofibers are not simply touching at the junction but indeed fused together. The statistics from more than 100 SEM images indicate that 72% of the junctions in Cu nanofiber networks were melted together. In comparison, previously reported CNTs or Ag nanowires tend to have higher junction resistances because they do not have the melt soldering effect.[9,15,17] Melt junctions between Cu nanofibers also result in less roughness compared to Ag nanowires, which reduces the probability of electrical shorting through devices fabricated on top of the electrode.[2]

Third, it has been shown that electrospinning can provide a facile process to align nanofibers to form regular arrays.[25] Here, we explore this capability for transparent electrodes to provide additional control on reducing the network resistance and manipulating optical polarization. Percolation theory predicts that aligning objects such as 1D nanostructures anisotropically can reduce the percolation threshold,[26] as shown in the case of CNTs.[26−28] By employing two metal strips separated by 1 cm (as shown schematically in Figure 1f), large scale Cu nanofiber arrays with uniform orientations and grid patterns can be fabricated across the two metal strips. The alignment is known to be driven by electrostatic interactions.[25] Panels g and h of Figure 1 show SEM images of Cu nanofiber arrays and patterns. In such directional nanomaterial systems, the charge carriers transport primarily along the fibers with little junction scattering. The nearly junction-free network with oriented nanofibers can greatly enhance the surface conductance in the orientation direction with a shorter conduction path compared with random network.[26] Moreover, these conductive nanofiber patterns also hold promising potential as large scale, low cost polarizers and touch screens.

To evaluate the performance of electrospun Cu nanofiber networks as transparent electrodes, the specular transmittance was measured. The density of Cu nanofiber networks can be easily controlled by adjusting the deposition time of the electrospinning process. As observed in Figure 2a, Cu nanofiber networks collected after different electrospinning times exhibit different transparencies. A four-probe method was used in sheet resistance measurements in order to avoid contact resistance between test electrodes and Cu nanofibers. The current−voltage curves of the nanofiber network (Figure 2b) are linear, indicating excellent Ohmic transport in the transparent Cu nanofiber network. The uniformity of the transparent electrode across the 5 cm by 2 cm sample was measured, and small variations of sheet resistance were observed (<10%). This result implies that the simple electrospinning process can be used for scaled-up fabrication of transparent electrodes with excellent film uniformity. Figure 2c shows the specular transmittance spectrum of a Cu nanofiber network. The random network of Cu nanofibers shows excellent optical transmittance in the visible and near-infrared ranges (300−1100 nm). Typically, 200 Ω/sq at ∼96%, 50 Ω/sq at ∼90%, and 12 Ω/sq at ∼80% can be achieved. As the density of Cu nanofibers increases, the sheet resistance decreases dramatically, which follows the percolation behavior of 1D stick systems.[7] Meanwhile, the transmittance decreases as the network thickness increases before reaching the effective skin depth of the metal network.[29] The transmittance losses with higher film thicknesses are mainly due to the increasing reflections, unlike the situations involving transparent CNTs, a fact which is confirmed from the large haze values as shown later. The resistance/transmittance ratio (R/T) performance with traditionally used ITO electrode on glass is compared to our Cu nanofiber network. As shown in Figure 2c, the ITO electrode shows a transmittance peak around 500 nm leading to a yellowish color. The yellowish color of ITO leads to a high color index value in lab color space which requires color adjustment components in displays.[5] By comparison, the Cu nanofiber network shows an excellent, flat spectrum in the whole measured range from 300 to 1100 nm. The flat spectrum, which can remove excess process steps and color adjustment components, is important for display applications. For solar cell applications, the transmittance in the near-infrared range is important because a significant amount of the solar energy falls into this region.[30] The flat transmittance spectrum can boost the application of transparent Cu electrodes in solar cells through utilization of the very broad solar spectrum wavelength range.

The performance of transparent Cu nanofiber networks is compared with traditional ITO electrodes, CNT networks, and graphene thin films, where specular transmittance is plotted against sheet resistance (Figure 2d). The major conclusions drawn from Figure 2d are the following: (1) The figure of merit, defined as $\Phi = T^{10}/R_s$ (Ω^{-1}), is normally used to evaluate the performance of the transparent electrodes near 90% transparency.[31] With the data shown in Figure 2d, the figure of merit is 11×10^{-3} Ω^{-1} for the Cu nanofiber network, 5×10^{-3} Ω^{-1} for ITO, 3.6×10^{-3} Ω^{-1} for CNTs, 0.4×10^{-3} Ω^{-1} for graphene, 5.6×10^{-3} Ω^{-1} for Ag

DOI: 10.1021/nl102725k | Nano Lett. 2010, 10, 4242–4248

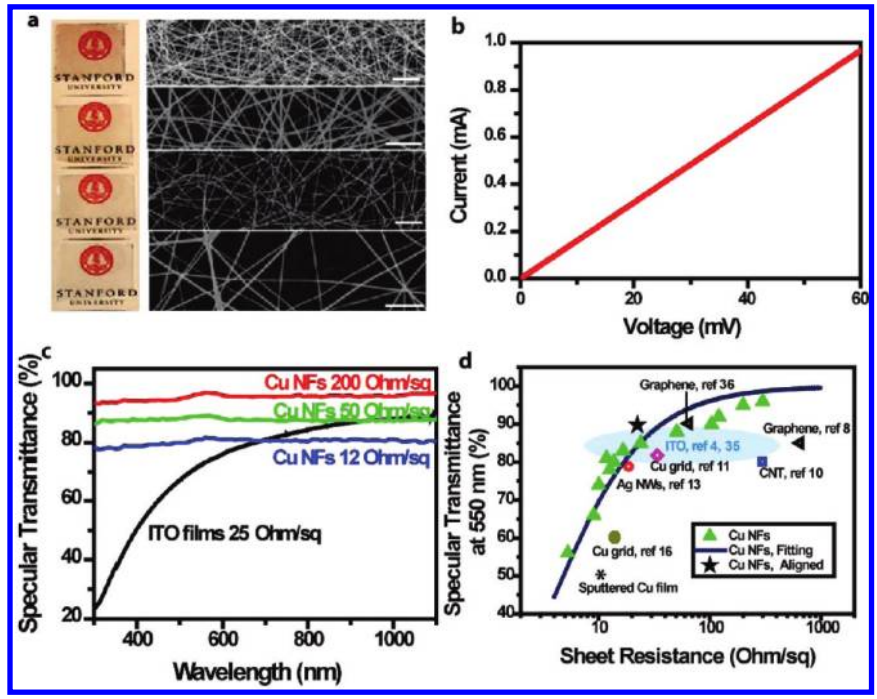

FIGURE 2. (a) Digital photos of a series of Cu nanofiber transparent electrodes with different fiber densities. Each sample has a size of 2 cm by 2.5 cm. The right column shows corresponding SEM images. Scale bar is 2 μm. (b) $I-V$ curve of Cu nanofiber thin film with a transparency of 85%. (c) Transmittance spectrum of Cu nanofiber webs with different sheet resistances and ITO on glass. The spectra for Cu nanofiber webs are much flatter than that of ITO films. (d) Performance comparison of our transparent Cu nanofiber network with a CNT network, graphene thin film, ITO electrode, Ag NW network, Cu grid, and sputtered Cu film with thickness of 50 nm. The solid line is for eye guiding.

nanowire networks, $0.5 \times 10^{-3}\ \Omega^{-1}$ for the Cu grid, and $0.1 \times 10^{-3}\ \Omega^{-1}$ for sputtered Cu films. A random network of Cu nanofibers outperforms all the other transparent electrodes in terms of sheet resistance and optical transmittance. (2) Cu nanofiber networks show better performance than sputtered Cu films on plastic substrates. Thin metal films on substrates normally show thickness dependent conductivities which are sensitive to surface defects and impurities. (3) Aligned Cu nanofiber networks increase the figure of merit of the transparent electrode even further, which is consistent with observations in CNT networks.[26] In Figure 2d, the black star indicates aligned cross arrays of Cu nanofibers, which show 90% transmittance at lower sheet resistances of 25 Ω/sq. In the oriented fiber networks, the resistances in the direction normal to the fibers are much higher than those along the fiber directions, typically >10000 times. In contrast with Cu grids fabricated by a nanoimprinting method which potentially can lead to anisotropic transparent electrodes, our electrospinning process is more suitable for scalable transparent electrodes with anisotropic surface conductance.

For transparent Cu nanofiber networks used in solar cell applications, the diffusive transmittance should be used instead of specular transmittance.[32] Similarly to the Ag NW system,[16,17] the transparent Cu nanofiber electrodes also show higher diffusive transmittances than specular transmittances. The difference between the diffusive transmittance and the specular transmittance is 10% at the ~80% specular transmittance and 4% at ~90% specular transmittance (Figure 3a). When diffusive transmittance is used, the figure of merit for the Cu nanofiber network is $23 \times 10^{-3}\ \Omega^{-1}$, much higher than the value, $5 \times 10^{-3}\ \Omega^{-1}$, for commercial ITO electrodes. Additionally, the large scattering of the metal nanofibers can enhance the solar cell performance due an effective increase in the light absorption path length in the active layer.[32] Note that due to the smooth surface of ITO, the specular and diffusive transmittance show negligible differences, much lower than Cu nanofibers network. Figure 3b shows the current−voltage data for an organic solar cell using Cu nanofiber networks as the transparent anode. The device fabrication and characterization details can be found in the Supporting Information. The power conversion efficiency of the device is 3.0%, which is comparable to devices made on glass/ITO substrates. The figures of merit for the device using a glass/Cu nanofiber substrate (J_{SC} 10.4 mA/cm^2, V_{OC} 0.55 V, FF 0.53) are comparable to a device using glass/ITO as the substrate (J_{SC} 10.3 mA/cm^2, V_{OC} 0.53 V, FF 0.66, power conversion efficiency 3.6%) with the exception of the lower fill factor (FF). The lower FF is the result of higher series resistance, which is the result of the sulfonic acid in PEDOT:PSS partially corroding the Cu nanofiber network during spin coating. After drying, Cu nanofibers are not exposed to acid anymore, and the etching of Cu nanofibers were stopped. Dried PEDOT:PSS could function as the protection layer; as a result, the Cu nanofibers were stable after spin coating. For the device shown in Figure

DOI: 10.1021/nl102725k | Nano Lett. 2010, 10, 4242–4248

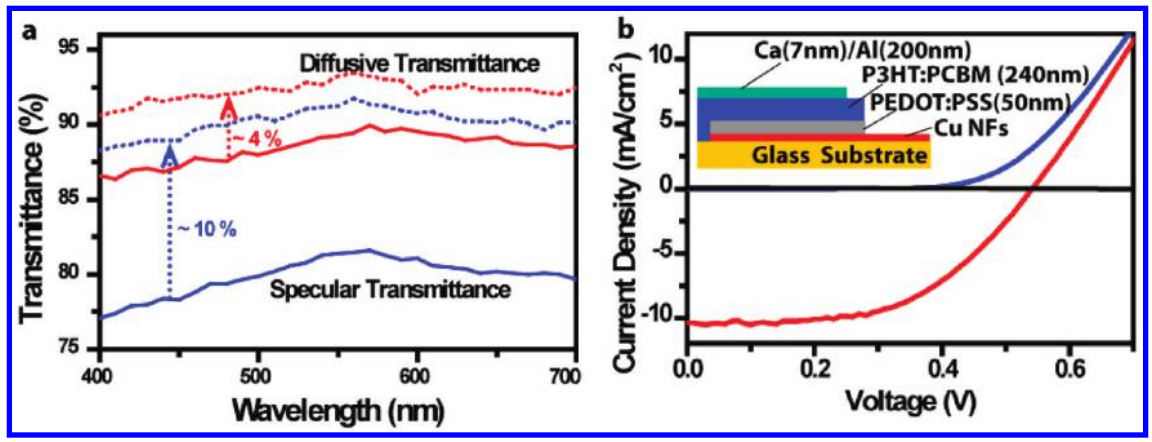

FIGURE 3. (a) Diffusive transmittance (dashed lines) is higher than specular transmittance (solid lines) in Cu nanofiber electrodes, which is beneficial for solar cell applications. Blue and red curves are for two networks with different densities. (b) Current−voltage data for a P3HT:PCBM solar cell using a Cu nanofiber film as the transparent electrode under AM1.5G conditions. The device is 1 × 5 mm and the device stack is glass/Cu nanofiber/PEDOT:PSS (50 nm)/P3HT:PCBM (240 nm)/Ca (7 nm)/Al (200 nm).

3b, R_s increased from ~35 to ~80 Ω/sq after the deposition of PEDOT:PSS, after which R_s was stable. Figure S7 (Supporting Information) show SEM images of Cu nanofibers after spin coating of PEDOT:PSS and stored for 1 week, indicating the stability of Cu nanofibers after acid drying. Work has already been done to replace the PEDOT:PSS layer in organic solar cells,[33] which is thought to have deleterious effects on the stabilities of organic solar cells. The effect on power conversion efficiency seen here could be a straightforward consequence of the increased R_s and should be eliminated with the eventual replacement of PEDOT:PSS with a noncorrosive layer. It is also worth commenting on the sheet resistance associated with transport within the PEDOT:PSS layer in the open spaces between the Cu nanofibers,[14] which is typically less than 10 μm even for films that are 90% transparent. The negative effect of sheet resistance on the power conversion efficiency scales as $R_s w$,[2] where w is the relevant length scale such as the device width or the greatest distance to a Cu nanofiber, which in this case are approximately 1 cm or 10 μm, respectively. For these two different length scales, w^2 differs by a factor of 10^6, and thus the sheet resistance requirements of the nanofiber network and the PEDOT:PSS also differ by a factor of 10^6. The sheet resistance of the PEDOT:PSS layer used here was 10^5 Ω/sq and thus should be more than conductive enough. It is also notable that there are negligible shorting effects even though the nanofiber network is rough relative to typical ITO films and the organic layer is very thin, ~240 nm. The electrospinning process naturally results in a network in which the fibers themselves are smooth and no wires can ever stick up out of the film. We believe this allows the organic layers to make a relatively conformal coating over the wires.

One concern related to Cu nanofibers is their chemical stability against oxidation in air. It is well-known that Cu will form oxides when exposed to air. In our study, we found that bare Cu nanofiber networks in air degraded slowly over a long time scale. For example, a Cu nanofiber transparent electrode kept undere ambient conditions for 3 months showed a sheet resistance increase from 10 to 18 Ω due to slow Cu oxidation, but the transparency showed no measurable change. For device applications, where Cu nanofibers are embedded underneath the other materials (e.g., Figure 3b), the chemical stability of Cu nanofibers is less of a concern. For the applications where Cu nanofibers are exposed to ambient atmosphere, a common practice of encapsulation is needed to increase long-term stability.

Due to their large aspect ratios, nanoscale diameters, and metallic bonding natures of Cu nanofibers, such transparent electrodes should show excellent flexibilities and stretching abilities. Transparent Cu nanofiber electrodes on poly(dimethylsiloxane) (PDMS) substrates are successfully fabricated by simply transferring free-standing CuO nanofiber networks to PDMS. The CuO network on PDMS is heated in an H_2 atmosphere at 300 °C to transform into Cu. The *T*/*R* performance of Cu nanofiber on PDMS remains the same with Cu nanofiber network on glass substrate (supplementary Figure S8, Supporting Information), indicating that the transfer process does not damage the nanofiber networks. These Cu nanofiber networks show excellent flexibilities. As shown in the inset of Figure 4a, Cu nanofiber electrode on PDMS substrate can be bent down to a 6 mm radius of curvature with little sheet conductance degradation. By comparison, Cu thin films on PDMS with the same sheet resistances (20 nm thick Cu, 9.2 ohm/sq, 50% specular transmittance) show nearly 2 orders of magnitude resistance increases upon bending to 6 mm radii. Indeed, the Cu thin films exhibit catastrophic failure when bent to an 8 mm radius. The failure is due to the cracking of the Cu film caused by large strain, as also commonly observed in ITO electrodes. SEM images (Figure 4c,d) show the film morphologies after the bending test for Cu nanofiber networks and Cu thin films on PDMS, respectively. Cu nanofibers maintain their 1D structure due to their large aspect ratios and small diameters, while Cu films form many cracks with gaps of

DOI: 10.1021/nl102725k | *Nano Lett.* **2010,** *10,* 4242–4248

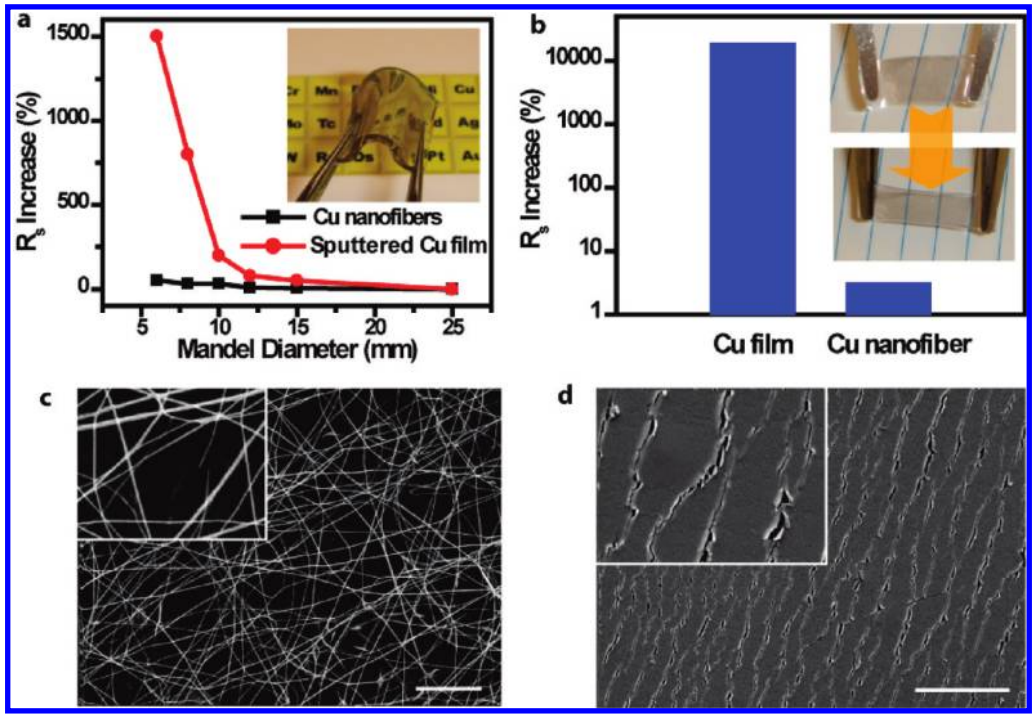

FIGURE 4. (a) The transparent electrodes based on Cu nanofiber networks show much better flexibilities than sputtered Cu films on PDMS substrates. The Mandrel diameter is the bending radius. (b) Cu nanofiber networks show much smaller changes in terms of sheet resistance upon stretching with 10% strain. The sheet resistance was measured after the films were released back to their original lengths. (c) An SEM image of a Cu nanofiber network after bending to a 6 mm radius indicates the fiber network structure is maintained. Scale bar = 10 μm. (d) An SEM image of Cu sputtered on PDMS after bending to a 6 mm radius clearly shows that the substrate breaks with large cracks. Scale bar = 10 μm.

~50 nm. For emerging applications, stretchable electrodes are needed when arbitrary shape transformations are required. The large aspect ratios of Cu nanofibers allow them to maintain their continuous network structures for conductance while releasing the strain built up during stretching. For the stretch test, a silver film was painted on both ends. The resistance was measured before and after the stretching test. Figure 4b shows the comparison of the relative changes of the resistance for Cu thin films (~50 nm thick) and Cu nanofiber network after the mechanical stretch test with 10% strain. Cu nanofiber networks show superior performance when compared to the Cu thin films. Cu nanofiber networks exhibit little conductance degradation after stretching to 10% strain, while the resistance for Cu thin films increases by 100 times. The excellent flexibilities and stretchabilities for the Cu nanofiber networks paves the way for emerging flexible or/and stretchable electronics as well.

In conclusion, continuous metal nanofibers with both random and aligned distributions were fabricated with the electrospinning process. These nanofiber networks are excellent transparent electrode materials, with performances superior to the reported transparent electrodes so far in terms of transmittance and sheet resistance. Furthermore, the mechanical flexibilities of the nanofiber network on plastic substrates are robust due to their large aspect ratios. The electrospinning method was also demonstrated to be a unique approach in fabricating aligned transparent conductors with anisotropic conductivities. All of these advantages should continue to expand and open up new applications.

Acknowledgment. Y.C. acknowledges support from the King Abdullah University of Science and Technology (KAUST) Investigator Award (No. KUS-l1-001-12), US Department of Energy, and Stanford Global Climate Energy Projects. J.M. acknowledges support from the National Science Foundation and National Defense Science and Engineering graduate research fellowships.

Supporting Information Available. Experimental procedure and additional figures. This material is available free of charge via the Internet at http://pubs.acs.org.

REFERENCES AND NOTES

(1) Hu, L.; Hecht, D.; Gruner, G. *Chem. Rev.* **2010**, ASAP.
(2) Rowell, M. W.; Topinka, M. A.; McGehee, M. D.; Prall, H. J.; Dennler, G.; Sariciftci, N. S.; Hu, L. B.; Gruner, G. *Appl. Phys. Lett.* **2006**, *88* (23), .
(3) Wyeth, N. C. *Solid-State Electron.* **1977**, *20* (7), 629–634.
(4) www.cpfilms.com.
(5) Leterrier, Y.; Medico, L.; Demarco, F.; Manson, J. A. E.; Betz, U.; Escola, M. F.; Olsson, M. K.; Atamny, F. *Thin Solid Films* **2004**, *460* (1−2), 156–166.
(6) Kumar, A.; Zhou, C. W. *ACS Nano* **2010**, *4* (1), 11–14.
(7) Hu, L.; Hecht, D. S.; Gruner, G. *Nano Lett.* **2004**, *4* (12), 2513–2517.
(8) Kim, K. S.; Zhao, Y.; Jang, H.; Lee, S. Y.; Kim, J. M.; Kim, K. S.; Ahn, J. H.; Kim, P.; Choi, J. Y.; Hong, B. H. *Nature* **2009**, *457* (7230), 706–710.

DOI: 10.1021/nl102725k | *Nano Lett.* **2010,** *10,* 4242–-4248

(9) Wu, Z. C.; Chen, Z. H.; Du, X.; Logan, J. M.; Sippel, J.; Nikolou, M.; Kamaras, K.; Reynolds, J. R.; Tanner, D. B.; Hebard, A. F.; Rinzler, A. G. *Science* **2004**, *305* (5688), 1273–1276.
(10) Li, J.; Hu, L.; Wang, L.; Zhou, Y.; Gruner, G.; Marks, T. J. *Nano Lett.* **2006**, *6* (11), 2472–2477.
(11) Eda, G.; Fanchini, G.; Chhowalla, M. *Nat. Nanotechnol.* **2008**, *3* (5), 270–274.
(12) Zhang, M.; Fang, S. L.; Zakhidov, A. A.; Lee, S. B.; Aliev, A. E.; Williams, C. D.; Atkinson, K. R.; Baughman, R. H. *Science* **2005**, *309* (5738), 1215–1219.
(13) Kang, M. G.; Kim, M. S.; Kim, J. S.; Guo, L. J. *Adv. Mater.* **2008**, *20* (23), 4408–4413.
(14) Tvingstedt, K.; Inganas, O. *Adv. Mater.* **2007**, *19* (19), 2893.
(15) Lee, J. Y.; Connor, S. T.; Cui, Y.; Peumans, P. *Nano Lett.* **2008**, *8* (2), 689–692.
(16) De, S.; Higgins, T. M.; Lyons, P. E.; Doherty, E. M.; Nirmalraj, P. N.; Blau, W. J.; Boland, J. J.; Coleman, J. N. *ACS Nano* **2009**, *3* (7), 1767–1774.
(17) Hu, L.; Kim, H. S.; Lee, Y. J.; Peumans, P.; Cui, Y. ACS Nano. 2010, ASAP.
(18) Kang, M. G.; Guo, L. J. *J. Vac. Sci. Technol., B* **2007**, *25* (6), 2637–2641.
(19) Li, D.; Xia, Y. N. *Adv. Mater.* **2004**, *16* (14), 1151–1170.
(20) Greiner, A.; Wendorff, J. H. *Angew. Chem., Int. Ed.* **2007**, *46* (30), 5670–5703.
(21) Bognitzki, M.; Becker, M.; Graeser, M.; Massa, W.; Wendorff, J. H.; Schaper, A.; Weber, D.; Beyer, A.; Golzhauser, A.; Greiner, A. *Adv. Mater.* **2006**, *18* (18), 2384.
(22) Li, D.; Xia, Y. N. *Nano Lett.* **2003**, *3* (4), 555–560.
(23) Wu, H.; Zhang, R.; Liu, X. X.; Lin, D. D.; Pan, W. *Chem. Mater.* **2007**, *19* (14), 3506–3511.
(24) Seager, C. H.; Pike, G. E. *Phys. Rev. B* **1974**, *10* (4), 1435–1446.
(25) Li, D.; Wang, Y. L.; Xia, Y. N. *Nano Lett.* **2003**, *3* (8), 1167–1171.
(26) Du, F. M.; Fischer, J. E.; Winey, K. I. *Phys. Rev. B* **2005**, *72* (12), .
(27) Kocabas, C.; Pimparkar, N.; Yesilyurt, O.; Kang, S. J.; Alam, M. A.; Rogers, J. A. *Nano Lett.* **2007**, *7*, 1195–1202.
(28) Behnam, A.; Ural, A. *Phys. Rev. B* **2007**, *75*.
(29) Kittle, C. *Introduction to Solid State Physics*; Wiley: New York, 1996.
(30) Strumpel, C.; McCann, M.; Beaucarne, G.; Arkhipov, V.; Slaoui, A.; Svrcek, V.; del Canizo, C.; Tobias, I. *Sol. Energy Mater. Sol. Cells* **2007**, *91* (4), 238–249.
(31) Yang, Y.; Wang, L.; Yan, H.; Jin, S.; Marks, T. J.; Li, S. Y. *Appl. Phys. Lett.* **2006**, *89* (5), .
(32) Atwater, H. A.; Ploman, A. *Nat. Mater.* **2010**, *9*, 205–213.
(33) Irwin, M. D.; Buchholz, B.; Hains, A. W.; Chang, R. P. H.; Marks, T. J. *Proc. Natl. Acad. Sci. U.S.A.* **2008**, *105* (8), 2783–2787.
(34) Li, G.; Shrotriya, V.; Huang, J. S.; Yao, Y.; Moriarty, T.; Emery, K.; Yang, Y. *Nat. Mater.* **2005**, *4* (11), 864–868.
(35) http://www.delta-technologies.com/.
(36) Bae, S.; Kim, H.; Lee, Y.; Xu, X.; Park, J. S.; Zheng, Y.; Balakrishnan, J.; Lei, T.; Kim, H. R.; Song, Y. I.; Kim, Y. J.; Kim, K. S.; Ozyilmaz, B.; Ahn, J. H.; Hong, B. H.; Iijima, S. *Nat. Nanotechnol.* **2010**, *5* (8), 574–578.

DOI: 10.1021/nl102725k | *Nano Lett.* **2010,** *10,* 4242–-4248